Wang *et al. Biochar* (2026) 8:144
https://doi.org/10.1007/s42773-026-00661-5

Biochar

ORIGINAL RESEARCH Open Access

Cell-wall chemistry governs anisotropic shrinkage during wood carbonization: roles of polysaccharide degradation and exchangeable cations

Yu Wang[1], Ramadan Eljamal[1], Misao Yokoyama[1], Takashi Nomura[1], Eiji Minami[1] and Haruo Kawamoto[1*]

Abstract

The anisotropic shrinkage of wood during carbonization critically affects biochar microstructure, but its underlying mechanisms remain unclear. We examined shrinkage behavior in the radial (R) and longitudinal (L) directions in relation to polysaccharide thermal degradation, exchangeable cation species, and cell structure, using ten wood species (five softwoods and five hardwoods) and their cation-exchanged derivatives (H^+, Na^+, K^+, Mg^{2+}, Ca^{2+}). Thermogravimetric and continuous dimensional analyses revealed that the onset of shrinkage in the R-direction is primarily associated with hemicellulose degradation, whereas shrinkage in the L-direction is linked to cellulose degradation and occurs rapidly at temperatures 10–20 °C higher than the derivative thermogravimetric peak, when most cellulose microfibrils have already decomposed. Na^+ and K^+ lowered shrinkage onset temperatures across most species, whereas in hardwoods, R-direction shrinkage magnitude increased with H^+ and Mg^{2+} substitution. Anatomical differences, particularly in ray parenchyma morphology, explained why hardwoods generally shrank more in the R direction. These results demonstrate that anisotropic shrinkage during wood carbonization is governed by polysaccharide-specific thermal degradation, modulated by exchangeable cation species and anatomical features. Furthermore, directional shrinkage can be predictably tuned through cation control and species selection to optimize biochar microstructure.

Highlights

- R-direction shrinkage begins with hemicellulose degradation and intensifies during cellulose degradation.
- L-direction shrinkage initiates with cellulose degradation and peaks as cellulose fully degrades.
- Shrinkage onset and extent are strongly affected by metal cations and wood cell structures.

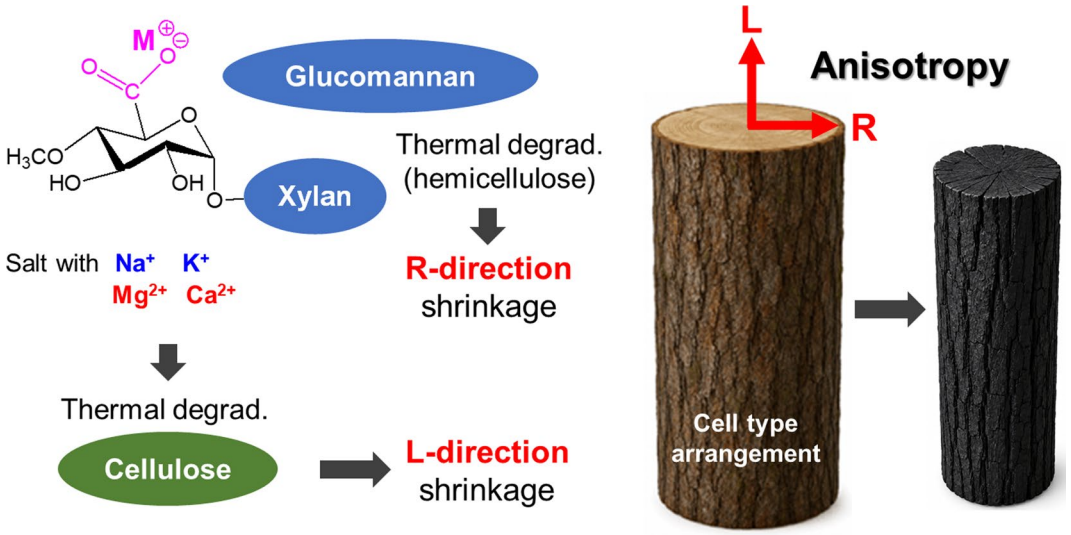
Keywords Wood cell wall chemistry, Thermogravimetric analysis, Exchangeable cations, Cellulose, Hemicellulose, Microstructure control

*Correspondence:
Haruo Kawamoto
kawamoto@energy.kyoto-u.ac.jp
Full list of author information is available at the end of the article

© The Author(s) 2026. **Open Access** This article is licensed under a Creative Commons Attribution 4.0 International License, which permits use, sharing, adaptation, distribution and reproduction in any medium or format, as long as you give appropriate credit to the original author(s) and the source, provide a link to the Creative Commons licence, and indicate if changes were made. The images or other third party material in this article are included in the article's Creative Commons licence, unless indicated otherwise in a credit line to the material. If material is not included in the article's Creative Commons licence and your intended use is not permitted by statutory regulation or exceeds the permitted use, you will need to obtain permission directly from the copyright holder. To view a copy of this licence, visit http://creativecommons.org/licenses/by/4.0/.

Springer

Graphical Abstract



1 Introduction

Wood has three principal anatomical directions: the longitudinal (L) direction, which runs parallel to the axis of the tree trunk; the radial (R) direction, which extends from the pith toward the bark and is perpendicular to the L direction; and the tangential (T) direction, which is perpendicular to both the L and R directions. These anatomical directions exhibit fundamentally different cell arrangements and cell wall architectures. In the L direction, most wood cells are aligned, and cellulose microfibrils are oriented along the cell axis. In contrast, ray parenchyma cells are aligned in the R direction, resulting in most cell lumina having their long axes oriented in the R direction and their short-axis cross-sections arranged in the L direction. At the cell wall level, cellulose microfibrils constitute the primary load-bearing framework and are embedded within a hemicellulose–lignin matrix. Xylan and glucomannan, the major hemicelluloses in hardwoods and softwoods, respectively, are generally associated with cellulose microfibril surfaces and contribute to the supramolecular structure of the cell wall. Therefore, wood exhibits anisotropy at both the cellular and cell wall levels.

Thermal degradation of cellulose, hemicellulose, and lignin thus proceeds within these anisotropic structural frameworks. The degradation behavior of these constituents is expected to determine the properties of wood-derived biochar at the macroscopic (wood), cellular, and cell wall levels, as well as its functional performance in applications such as adsorption, catalysis, and soil amendment (Wang and Howard 2017; Yu et al. 2018; de Oliveira et al. 2022; Wang et al. 2024). For example, dimensional stability and pore preservation are favorable for adsorption and catalysis, whereas controlled anisotropic shrinkage may enhance soil amendment performance by promoting microporosity. The R and L shrinkage behaviors differ markedly due to anisotropic cell arrangement and the heterogeneous thermal degradation of the constituent polysaccharides (Rafsanjani et al. 2014; Xue et al. 2018; Gao et al. 2022; Wang et al. 2024). However, the detailed mechanisms underlying these relationships remain unclear.

A previous study (Wang et al. 2024) has shown that the onset and progression of shrinkage in different anatomical directions are strongly linked to the thermal degradation behavior of hemicelluloses and cellulose. They demonstrated that, in untreated samples of ten softwood and hardwood species, R-direction shrinkage is closely associated with hemicellulose degradation, whereas L-direction shrinkage is primarily governed by cellulose degradation. That study, based solely on thermogravimetric (TG) analysis, further proposed that the onset temperature difference between the R and L directions (ΔT) correlates strongly with shrinkage anisotropy.

Subsequent work using the same ten species (Wang et al. 2025a, 2025b) provided the first evidence that alkali and alkaline earth metal cations, which are naturally present in wood and are mainly exchangeable with the uronic acid residues of xylan, profoundly influence

wood pyrolysis, particularly cellulose degradation. The results showed that Na^+ and K^+ substitution lowered the cellulose degradation temperature by approximately 30 °C, despite cellulose being the most thermally stable wood component. In contrast, these cations had only minor effects on xylan, while markedly altering glucomannan reactivity. TG-MS analysis of lignin pyrolysis behavior suggested that cations modify lignin's thermal degradation reactivity, which in turn affects both glucomannan and cellulose.

Building on previous work, the present study focuses on elucidating how exchangeable cation species, polysaccharide thermal reactivity, and anatomical features interact to determine anisotropic shrinkage, defined as uneven shrinkage of wood in different directions during heating, in wood carbonization. While earlier studies (Wang et al. 2025a, 2025b) quantified the thermal degradation reactivity of cellulose, glucomannan, and xylan for the same ten species, and the first report (Wang et al. 2024) directly monitored shrinkage behavior by TG analysis, the combined effects of cation species, wood anatomy, and polysaccharide chemistry on R- and L-direction shrinkage have not been systematically addressed.

In this study, both untreated and cation-exchanged woods from the same ten species (five softwoods and five hardwoods) were analyzed using previously obtained polysaccharide reactivity data in conjunction with continuous measurements of shrinkage in the R and L directions during heating. It is hypothesized that cation-induced changes in polysaccharide degradation reactivity, together with species-specific anatomical characteristics, govern the dimensional stability and structural evolution of biochar during carbonization. By correlating shrinkage onset and rate with the degradation behavior of cellulose, glucomannan, and xylan, the underlying mechanisms are elucidated. These findings provide new insights into wood carbonization and a scientific basis for process optimization and microstructural control in biochar production, while supporting the efficient and sustainable utilization of biomass resources within the environmental-economic nexus (Maroušek and Trakal 2022).

2 Materials and methods

2.1 Materials

Veneer sheets (thickness ≈ 0.2 mm) of five softwood species, namely Japanese cedar (*Cryptomeria japonica*), Japanese cypress (*Chamaecyparis obtusa*), western redcedar (*Thuja plicata*), Douglas fir (*Pseudotsuga menziesii*), and Japanese larch (*Larix leptolepis*), and five hardwood species, namely Japanese beech (*Fagus crenata*), Japanese zelkova (*Zelkova serrata*), walnut (*Juglans* spp.), ash (*Fraxinus* spp.), and paulownia (*Paulownia tomentosa*), were obtained from Daiwa Tsukiita Sangyo Corp. (Hiroshima, Japan). For each veneer, only the sapwood portion was used. These ten wood species were selected to represent commonly available and widely utilized softwood and hardwood species in Japan, covering a range of anatomical structures and chemical compositions. By including five softwoods and five hardwoods, we aimed to capture systematic differences in hemicellulose composition (e.g., glucomannan-rich softwoods and xylan-rich hardwoods), cell wall architecture, and exchangeable cation content. Japanese larch was also included as an exceptional softwood species containing a substantial amount of galactan, thereby allowing us to account for a distinctive variation in hemicellulose composition among the softwood species examined. All reagents including HCl and metal acetates were purchased from Nacalai Tesque, Inc. (Kyoto, Japan) and used without further purification.

Samples were first impregnated with 0.05 M HCl under vacuum using a wood-to-solution weight ratio of 1:20 (w/w), followed by 24 h soaking, to remove native mineral cations and replace them with protons (H^+). The resulting H^+-exchanged (demineralized) samples were rinsed with deionized water to neutral pH and dried. Cation exchange was then performed by immersing the dried samples in 0.05 M solutions of sodium acetate (98.5%), potassium acetate (97%), magnesium acetate tetrahydrate (99%), or calcium acetate monohydrate (99%) under vacuum, followed by 24 h soaking, replacing the carboxyl-bound protons with the corresponding metal cations. After rinsing to neutrality and drying, a total of 50 distinct samples were obtained, representing ten wood species each treated with five cation forms: H^+, Na^+, K^+, Mg^{2+}, and Ca^{2+}. Each sample was cut into approximately 4 mm × 4 mm slices along the longitudinal and radial directions for further analysis.

2.2 Methods

2.2.1 Thermogravimetric measurements

Thermogravimetric (TG) measurements were conducted using a thermal analyzer with a CCD camera (NEXTA STA200RV, Hitachi High-Tech Corp., Tokyo, Japan), as described in previous work (Wang et al. 2024). For each run, a 4 × 4 mm veneer sheet was placed in an aluminum pan and heated from 40 °C to 550 °C at 10 °C/min under a nitrogen flow of 100 mL/min, and the corresponding TG and derivative TG (DTG) profiles were recorded. CCD images captured during the TG runs were analyzed to determine longitudinal (L) and radial (R) dimensions at each set temperature, expressed relative to their values at 150 °C:

$$L = \frac{L_i}{L_{150}} \times 100(\%) \quad (1)$$

$$R = \frac{R_i}{R_{150}} \times 100(\%) \quad (2)$$

where L_i and R_i denote the lengths at a given temperature, and L_{150} and R_{150} those at 150 °C in the L and R directions, respectively.

The onset temperature of shrinkage was defined, for both longitudinal (Onset T(L)) and radial (Onset T(R)) directions, as the temperature at which shrinkage was first detected in each direction. Similarly, the temperatures at which the shrinkage rates in the radial and longitudinal directions reached their maxima were defined as Max T(R) and Max T(L), respectively.

2.2.2 Pyrolysis experiments

Pyrolysis was carried out using a high-frequency induction heating system (MU-α-III, SK Medical Electronics Co., Ltd., Japan), as described in previous work (Wang et al. 2025b). For each run, a veneer sheet (approximately 20 mg, 30 mm × 10 mm) was heated under a nitrogen flow of 100 mL min^{-1} in two sequential stages: (i) preheating from ambient temperature to 220 °C, and (ii) heating from 220 °C to the designated target temperature (240–400 °C, at 20 °C intervals). Upon reaching the target temperature, induction heating was immediately stopped to terminate pyrolysis, and the reactor was allowed to cool to room temperature under continuous nitrogen flow.

As the temperature increases, certain temperature ranges are particularly critical for interpretation. For example, temperature regions in which cellulose recovery decreases sharply are especially important for understanding degradation behavior. In contrast, temperature ranges where cellulose has already been almost completely decomposed are less informative for mechanistic discussion. Accordingly, we increased the number of replicates in temperature regions that are most relevant to the key conclusions of this study in order to ensure reproducibility and statistical reliability of these critical data points.

2.2.3 Hydrolysable sugar analysis

Hydrolysable sugars in the wood samples, before and after pyrolysis, were quantified via sulfuric acid hydrolysis. Detailed experimental procedures are provided in our previous study (Wang et al. 2025a). Xylan and glucomannan recovery rates were defined as the ratios of xylose and mannose contents after pyrolysis to those before pyrolysis, respectively. Cellulose recovery was estimated from the glucose yield, corrected by subtracting the glucomannan-derived glucose; for this calculation, the mannose-to-glucose ratio in glucomannan was assumed to be 3:1 for both softwoods and hardwoods. These recovery rates of hemicelluloses and cellulose were evaluated at each pyrolysis temperature.

2.2.4 Determination of metal cation contents

The specific method is as follows (Wang et al. 2025b): approximately 100 mg of each cation-exchanged sample was ashed in a muffle furnace at 600 °C for 6 h in air. The ash was dissolved in 30 mL of 0.1 M HNO_3 under sonication for 10 min, followed by filtration through a 0.45 μm membrane. Na^+, K^+, Mg^{2+}, and Ca^{2+} concentrations were quantified using inductively coupled plasma atomic emission spectroscopy (ICPE−9000, Shimadzu Corp., Kyoto, Japan), and the results are presented in Table S1.

3 Results

3.1 Shrinkage behavior of virgin and demineralized softwoods and hardwoods

In our previous study (Wang et al. 2024), shrinkage behavior of ten wood species was analyzed using only TG data. Here, we extend this work by including demineralized samples and examining the relationship between shrinkage anisotropy and the extent of decomposition of cellulose and hemicelluloses at the onset of shrinkage in the R and L directions. Figure 1 plots the recovery yields of cellulose, glucomannan, and xylan against the onset temperatures of shrinkage, previously defined as Onset T (R) and Onset T (L). The onset temperatures are shown on the x-axis. The recovery yields at these temperatures were presented in our previous paper (Wang et al. 2025a).

At Onset T (R), most of the cellulose remained undegraded, whereas 40–90% of glucomannan and 30–90% of xylan remained (except for Japanese cedar), although considerable interspecies variation was observed. This suggests that the onset of R-direction shrinkage is associated primarily with hemicellulose decomposition rather than cellulose decomposition. At Onset T (L), the percentages of glucomannan and xylan remaining were generally below 10–20% (except for Japanese cedar and ash), indicating that these hemicelluloses had undergone extensive decomposition. In contrast, 10–80% of the cellulose remained, indicating that L-direction shrinkage began only after cellulose decomposition had progressed substantially. These results are consistent with the hypotheses proposed in our previous TG-based study (Wang et al. 2024).

For the exceptional species, Japanese cedar and ash, the differences can be attributed to the high K^+ and Na^+ contents in these species (Wang et al. 2025b). As discussed below, these monovalent cations promote the co-degradation of cellulose and hemicelluloses. Consequently, cellulose degradation can proceed even while relatively large amounts of hemicelluloses remain, which may explain

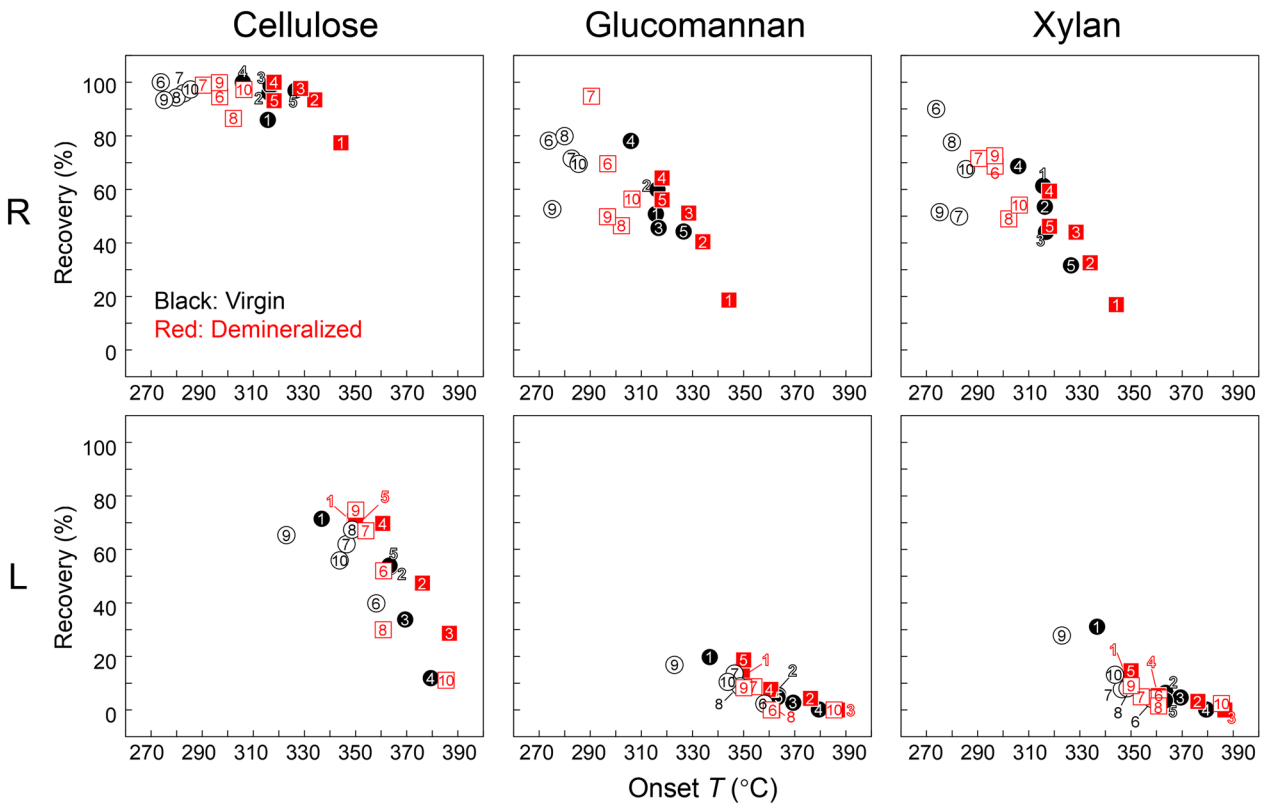


Fig. 1 Relationship between the recovery (%) of cellulose, glucomannan, and xylan, and shrinkage onset temperature in the R and L directions for virgin (black circles) and demineralized (red squares) softwood and hardwood species. Solid symbols: softwoods; Open symbols: hardwoods. 1: Japanese cedar; 2: Japanese cypress, 3: western redcedar; 4: Douglas fir; 5: Japanese larch; 6: Japanese beech; 7: Japanese zelkova; 8: Japanese walnut; 9: ash; 10: paulownia

why L-direction shrinkage begins at higher hemicellulose recovery yields in Japanese cedar and ash than in the other species. Upon demineralization, Onset *T* (L) shifted to higher temperatures, and the hemicellulose recovery yields at Onset *T* (L) decreased to levels comparable to those observed for the other species, further supporting the involvement of K^+ and Na^+ in their characteristic shrinkage behavior.

For the demineralized samples, the recovery yields of cellulose and hemicelluloses at the onset of shrinkage were generally similar to those of the untreated samples, whereas the onset temperatures tended to shift to higher temperatures. This shift is likely related to the removal of monovalent cations, particularly Na^+ and K^+, which promote the thermal decomposition of cellulose and glucomannan, as discussed in detail in Sect. 3.2.

Regarding interspecies differences, comparison between softwoods and hardwoods revealed no consistent difference in the longitudinal direction, where interspecies variation was more pronounced. In contrast, hardwoods generally showed lower Onset T (R) values than softwoods, with larger amounts of glucomannan and xylan remaining at the onset of radial shrinkage. Similar trends were observed for the demineralized samples.

3.2 Shrinkage behavior of metal cation exchanged softwoods and hardwoods

Our previous work with the same ten species (Wang et al. 2025b) demonstrated that the reactivity of the constituent polysaccharides, particularly cellulose and glucomannan, was primarily determined by the species of exchangeable cations, rather than by whether the wood was a softwood or hardwood. In the present study, we investigated the shrinkage behavior of wood samples exchanged with H^+, Na^+, K^+/Na^+, Mg^{2+}, and Ca^{2+}.

As noted in our previous report (Wang et al. 2025b), the potassium acetate reagent used for cation exchange contained sodium acetate as an impurity (0.5%). In many species, Na^+ uptake was not negligible, and in some cases, Na^+ incorporation even exceeded that of K^+. Because Na^+ and K^+ exert similar effects on the thermal degradation behavior of wood polysaccharides, we follow the convention of our previous study and designate

these samples as K^+/Na^+-exchanged wood throughout this paper.

Figure 2a and b show (i) shrinkage curves in the R and L directions, (ii) the R/L ratio as an index of shrinkage anisotropy, and (iii) shrinkage rate curves obtained by differentiating the shrinkage curves. Photographs of specimens during TG analysis are presented in Fig. S1.

Shrinkage began in the R direction, followed by the L direction (Figs. 2 and S1). As temperature increased, the R/L ratio declined gradually, then dropped sharply in the range where R-direction shrinkage accelerated. The ratio stabilized above ~400 °C, which is beyond the temperature of maximum L-direction shrinkage rate. As noted previously (Wang et al. 2024), the R/L ratio at 450 °C was proposed as a practical index of anisotropy during carbonization. The disappearance of anisotropy above 400 °C likely reflects the loss of cell-wall supramolecular structure, particularly that associated with cellulose microfibrils, which normally restrict L-direction shrinkage.

With few exceptions, Na^+ and K^+/Na^+ exchange led to shrinkage onset at lower temperatures than H^+, Mg^{2+}, or Ca^{2+} exchange in both R and L directions, reflecting the strong influence of cation species on thermal reactivity. Exceptions included Japanese larch, whose thermal reactivity and shrinkage curves were largely insensitive to cation type, and Japanese walnut, whose Mg^{2+}-exchanged wood exhibited higher thermal reactivity and correspondingly shifted shrinkage curves. These two species were also identified as exceptional in our previous study (Wang et al. 2025a, 2025b). The distinctive behavior of Japanese larch was attributed to its galactan-containing hemicellulose composition, whereas that of Japanese walnut was suggested to be related to a relatively less compact aggregation state of its cell-wall components.

Consistent with our previous findings (Wang et al. 2024), hardwoods generally showed greater R-direction shrinkage than softwoods, regardless of cation type, while L-direction shrinkage was about 90% across all species and cation types. The effect of cation species on R-direction shrinkage was most evident in hardwoods; for instance, Japanese beech and ash exchanged with Mg^{2+} or H^+ shrank more than those exchanged with other cations. In both wood groups, Ca^{2+} exchange tended to reduce R-direction shrinkage, though substantial species-specific variability was observed.

Among the hardwoods, Japanese zelkova consistently showed smaller R-direction shrinkage ratios. This trend persisted across the cation-exchanged samples and is likely due to the high calcium oxalate content in zelkova, much of which remains after cation exchange, allowing the influence of Ca to persist regardless of the exchanged cation.

Figure 3 summarizes the relationships between Onset *T* (R) or Onset *T* (L) and the residual percentages of cellulose, glucomannan, and xylan for H^+-, K^+/Na^+-, and Ca^{2+}-exchanged samples. Softwoods and hardwoods are plotted in blue and red, with open symbols for the R direction and solid symbols for the L direction. Because Na^+ resembled K^+/Na^+ and Mg^{2+} resembled Ca^{2+} in thermal behavior, only K^+/Na^+ and Ca^{2+} results are shown for clarity. Diagonal lines aid cross-comparison between graphs; a higher recovery yield at the onset temperature indicates that shrinkage in that direction begins at a less advanced stage of polysaccharide decomposition and thus reflects a greater tendency to shrink, whereas a lower recovery yield indicates that more extensive decomposition is required before shrinkage begins.

The recovery yields of polysaccharides at the onset of shrinkage in the R and L directions (Fig. 3) were generally consistent with those for virgin and demineralized wood (Fig. 1). R-direction shrinkage was linked to hemicellulose degradation, with onset recovery yields ranging from 20% to 90% for both glucomannan and xylan across all cations, though interspecies variation was substantial. Hardwood species typically had higher recovery yields than softwoods, a difference most pronounced for K^+/Na^+ and smallest for Ca^{2+}. In K^+/Na^+-exchanged hardwoods, except paulownia, the recovery yields at Onset *T* (R) reached 60–80% for glucomannan and 80–90% for xylan. These higher recovery yields indicate R-direction shrinkage began after less extensive hemicellulose decomposition than in wood exchanged with the other cations. Thus, in addition to promoting polysaccharide decomposition, K^+/Na^+ appears to enhance the tendency for R-direction shrinkage to occur at an earlier stage of hemicellulose decomposition.

Species-specific trends were also evident. Japanese cedar was generally less prone to R-direction shrinkage, with its H^+-exchanged sample showing a particularly low hemicellulose recovery yield at Onset *T* (R). Japanese zelkova exhibited unusually high recovery yields in H^+-exchanged samples, likely due to its persistent calcium oxalate content. Japanese beech showed consistently high glucomannan and xylan recovery yields at Onset *T* (R) for all cations, together with low Onset *T* (R) values, indicating a strong tendency toward R-direction shrinkage.

Consistent relationships between Onset T and recovery yields were generally observed across wood species for each cation type, most clearly for H^+- and Ca^{2+}-exchanged samples. This is consistent with our previous finding that polysaccharide reactivity is governed more strongly by the exchangeable cation species than by differences among wood species. For cellulose and glucomannan, the recovery–temperature relationships

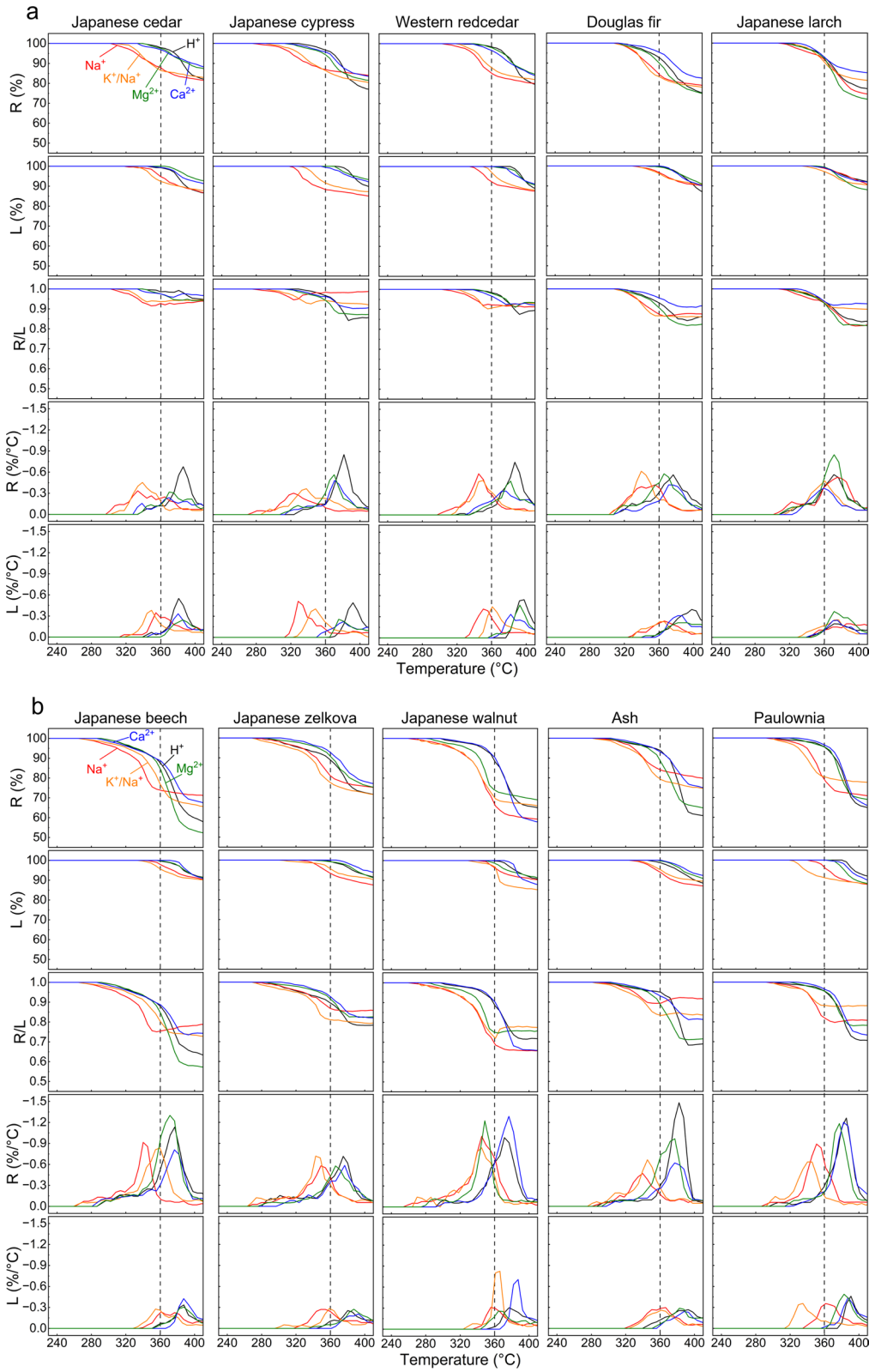


Fig. 2 Shrinkage curves in the R and L directions, R/L ratio curves and shrinkage rate curves in the R and L direction during thermogravimetric analysis for softwoods (**a**) and hardwoods (**b**) exchanged with H^+ (black), Na^+ (red), K^+/Na^+ (orange), Mg^{2+} (green), and Ca^{2+} (blue) ions

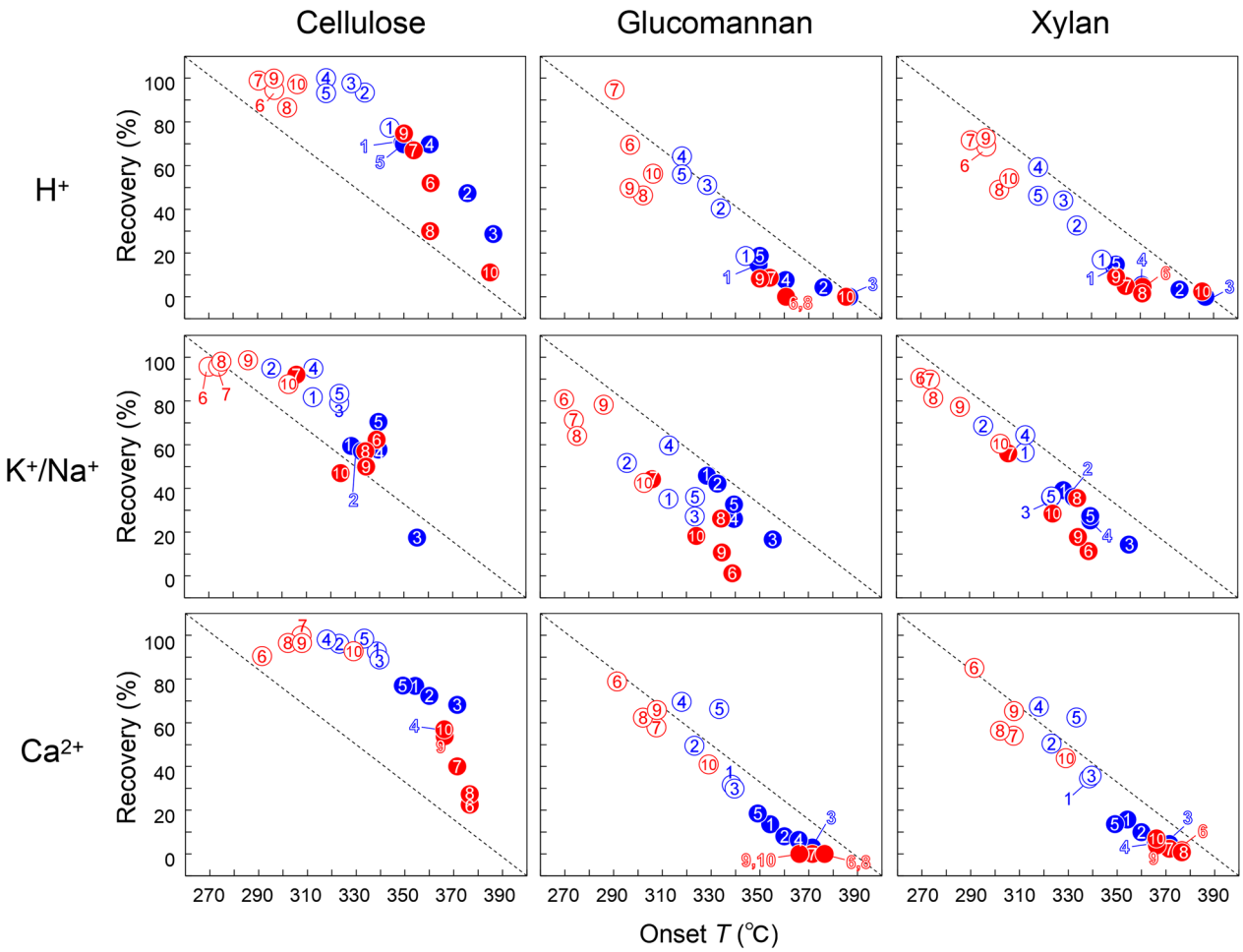


Fig. 3 Relationships between Onset *T* (R: open circles) and Onset *T* (L: solid circles), and the recovery yields of cellulose, glucomannan, and xylan for H^+-, Ca^{2+}-, and K^+/Na^+-exchanged softwood (blue) and hardwood (red) species. 1: Japanese cedar; 2: Japanese cypress, 3: western redcedar; 4: Douglas fir; 5: Japanese larch; 6: Japanese beech; 7: Japanese zelkova; 8: Japanese walnut; 9: ash; 10: paulownia

for K^+/Na^+-exchanged samples were shifted toward lower temperatures compared with those for H^+- and Ca^{2+}-exchanged samples, indicating enhanced thermal reactivity in the presence of K^+/Na^+. For glucomannan, this shift was particularly pronounced in hardwoods, resulting in greater scatter in the K^+/Na^+ plots. In contrast, no comparable shift was observed for xylan.

Onset *T* (L) corresponded to the temperature range where cellulose recovery dropped sharply, reflecting the role of longitudinally aligned cellulose microfibrils in resisting L-direction shrinkage. The lower Onset *T* (L) of K^+/Na^+-exchanged samples is therefore consistent with the enhanced thermal reactivity of cellulose in the presence of these monovalent cations.

The hemicellulose recovery yield at Onset *T* (L) varied with cation species, being generally higher in K^+/Na^+-exchanged samples. This can be explained by the co-degradation of cellulose and hemicelluloses: in the presence of K^+/Na^+, partial cellulose degradation begins at lower temperatures where hemicellulose degradation primarily occurs, allowing L-direction shrinkage to begin while relatively large amounts of hemicelluloses remain (Wang et al. 2025b). In contrast, samples exchanged with H^+, Ca^{2+}, or Mg^{2+} showed more independent degradation of cellulose and hemicelluloses (Wang et al. 2025b).

Because cellulose decomposition is most pronounced near the DTG peak temperature (T_p), Fig. 4 plots Onset *T* (L) against T_p for each cation species, with the range for virgin wood (excluding ash) highlighted. Across all species, Onset *T* (L) occurred slightly below or near T_p, further supporting the close association between L-direction shrinkage and cellulose decomposition. Cellulose recovery yields at T_p (Tables 1 and S2) were determined from temperature-dependent degradation curves by identifying the residual cellulose fraction at the specified temperatures. These yields ranged

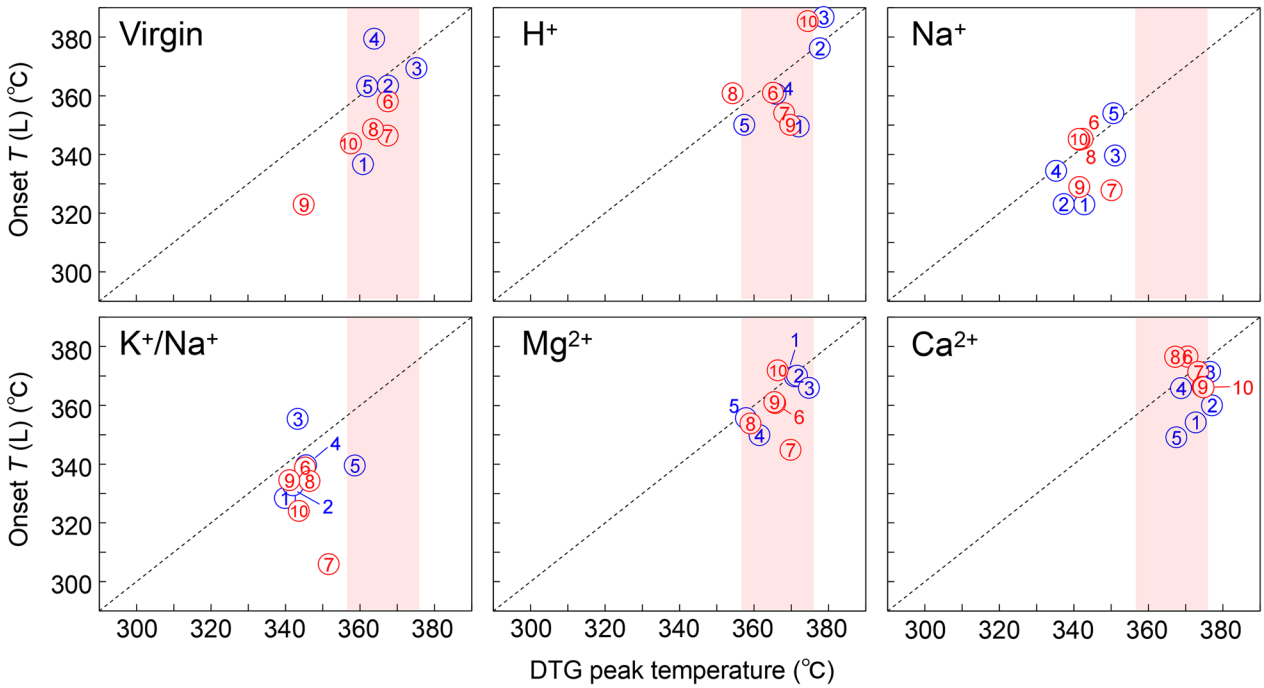


Fig. 4 Relationship between onset *T* (L) and DTG peak temperature of cation-exchanged softwood and hardwood species compared with the range for virgin wood (excluding ash), highlighted by a red shadow square. Blue: softwoods; red: hardwoods; 1: Japanese cedar; 2: Japanese cypress, 3: western redcedar; 4: Douglas fir; 5: Japanese larch; 6: Japanese beech; 7: Japanese zelkova; 8: Japanese walnut; 9: ash; 10: paulownia

Table 1 Cellulose recovery yields (%) at *Tp*, *Tp* + 10°C and *Tp* + 20°C of softwoods and hardwoods

Softwoods				**Hardwoods**			
Type	**T_p※**	**T_p + 10°C**	**T_p + 20°C**	**Type**	**T_p**	**T_p + 10°C**	**T_p + 20°C**
Virgin	19–57	5–36	2–16	Virgin	25–41	6–20	1–7
H^+	29–56	9–35	3–16	H^+	30–42	8–25	2–6
K^+/Na^+	27–42	14–21	2–8	K^+/Na^+	34–54	12–17	2–12
Ca^{2+}	30–49	10–22	3–10	Ca^{2+}	28–44	6–18	2–7

※: T_p is defined as the peak temperature of the derivative thermogravimetric curve obtained from thermogravimetric analysis

from 19% to 57% for softwoods and from 25% to 54% for hardwoods, consistent with the cellulose recovery yields observed at Onset *T* (L) in Fig. 3.

As noted earlier, the thermal degradation temperature of cellulose depends on the cation species, with Onset *T* (L) generally occurring at lower temperatures for Na^+- and K^+/Na^+-exchanged samples than for those exchanged with H^+, Mg^{2+}, or Ca^{2+}. This cation effect also explains the exceptionally low Onset *T* (L) of virgin ash compared with the other virgin wood samples: its high Na^+ and K^+ contents likely promote cellulose degradation at lower temperatures, thereby shifting the onset of L-direction shrinkage to lower temperatures. In other species, including Japanese cedar, the effect on Onset *T* (L) was minimal despite its high Na^+ and K^+ contents, probably because the influence of its relatively high Ca^{2+} content outweighed that of Na^+ and K^+.

As shown in Fig. 3, Onset *T* (L) exhibited no clear difference between softwoods and hardwoods for any cation species, whereas Onset *T* (R) was distinctly lower in hardwoods. Consequently, the difference between the onset temperatures in the two directions, ΔT = Onset *T* (L) – Onset *T* (R), tended to be larger in hardwoods than in softwoods. Our previous work (Wang et al. 2024) reported a strong correlation between ΔT and shrinkage anisotropy at 450 °C (R/L ratio) for the ten virgin wood species. To examine whether this relationship also applies to wood with different exchangeable

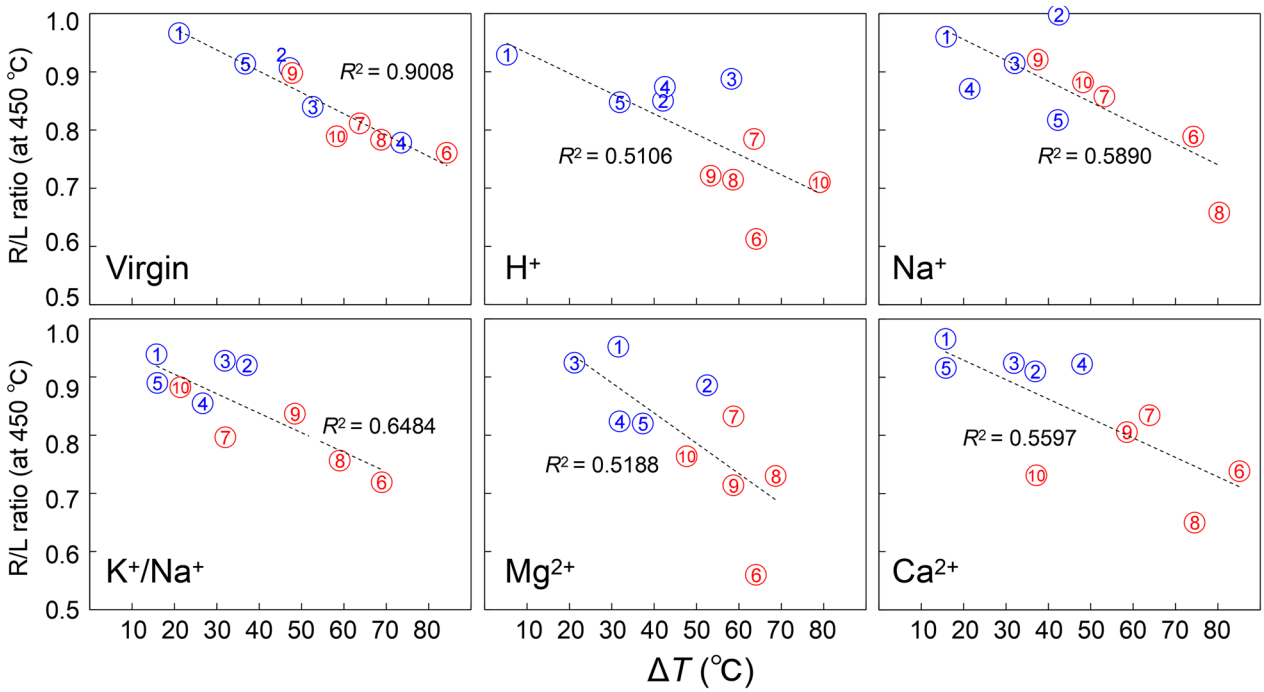


Fig. 5 Relationship between Δ*T* and R/L ratio at 450 °C. 1: Japanese cedar; 2: Japanese cypress; 3: western redcedar; 4: Douglas fir; 5: larch; 6: Japanese beech; 7: Japanese zelkova; 8: walnut; 9: ash; 10: paulownia. Blue: softwoods; red: hardwoods. Δ*T*: Onset *T* (L) – Onset *T* (R). R/L ratio (450 °C): ratio of the lengths in the R and L directions at 450 °C

cations, Fig. 5 presents the relationship between Δ*T* and the R/L ratio for the cation-exchanged samples, together with the virgin wood data from our previous study.

In the cation-exchanged samples, Δ*T* was generally smaller in softwoods than in hardwoods. As observed for virgin wood, a larger Δ*T* was associated with a lower R/L ratio at 450 °C, indicating greater shrinkage anisotropy. Although this negative correlation was still evident in the cation-exchanged samples, the variation among species was greater than that observed for virgin wood. Accordingly, the R^2 values for the linear regressions decreased from 0.9008 for virgin wood to 0.5106–0.6484 for the cation-exchanged samples.

Figures 6a and b plot the temperatures at which the shrinkage rates reach their maxima, defined as Max *T* (R) and Max *T* (L), against the DTG peak temperature (T_p). The solid diagonal line indicates Max $T = T_p$, while the dashed line represents Max $T = T_p + 20$ °C for reference.

In most cation-exchanged samples, Max *T* (R) generally coincided with T_p. Although cells aligned in the R direction are mostly ray parenchyma cells and constitute only a small proportion of the wood tissue, R-direction shrinkage progressed substantially near T_p, where cellulose degradation is pronounced. This suggests that the cellulose microfibrils of these cells also contribute to resistance against shrinkage in the R direction.

In contrast, in H^+- and Mg^{2+}-exchanged samples, Max *T* (R) occurred on average about 10 °C above T_p, and was accompanied by greater R-direction shrinkage. The cellulose recovery yields at T_p + 10 °C for H^+-exchanged samples ranged from 9% to 35% in softwoods and 8–25% in hardwoods (Table 1). These relatively low yields suggest that more extensive thermal degradation of cellulose is required to induce significant R-direction shrinkage in H^+- and Mg^{2+}-exchanged wood than in Na^+-, K^+/Na^+-, or Ca^{2+}-exchanged wood. The tendency toward independent degradation of cellulose and hemicelluloses observed in H^+- and Mg^{2+}-exchanged wood may be related to this phenomenon; however, further investigation is required to clarify the underlying mechanism.

Max *T* (L) occurred approximately 10 °C higher than Max *T* (R), corresponding to T_p + 10–20 °C, at which cellulose degradation had progressed extensively (cellulose recovery yields: 2–36% in softwoods, 1–25% in hardwoods; Table 1). This indicates that efficient L-direction shrinkage requires extensive degradation of cellulose microfibrils, suggesting that the remaining

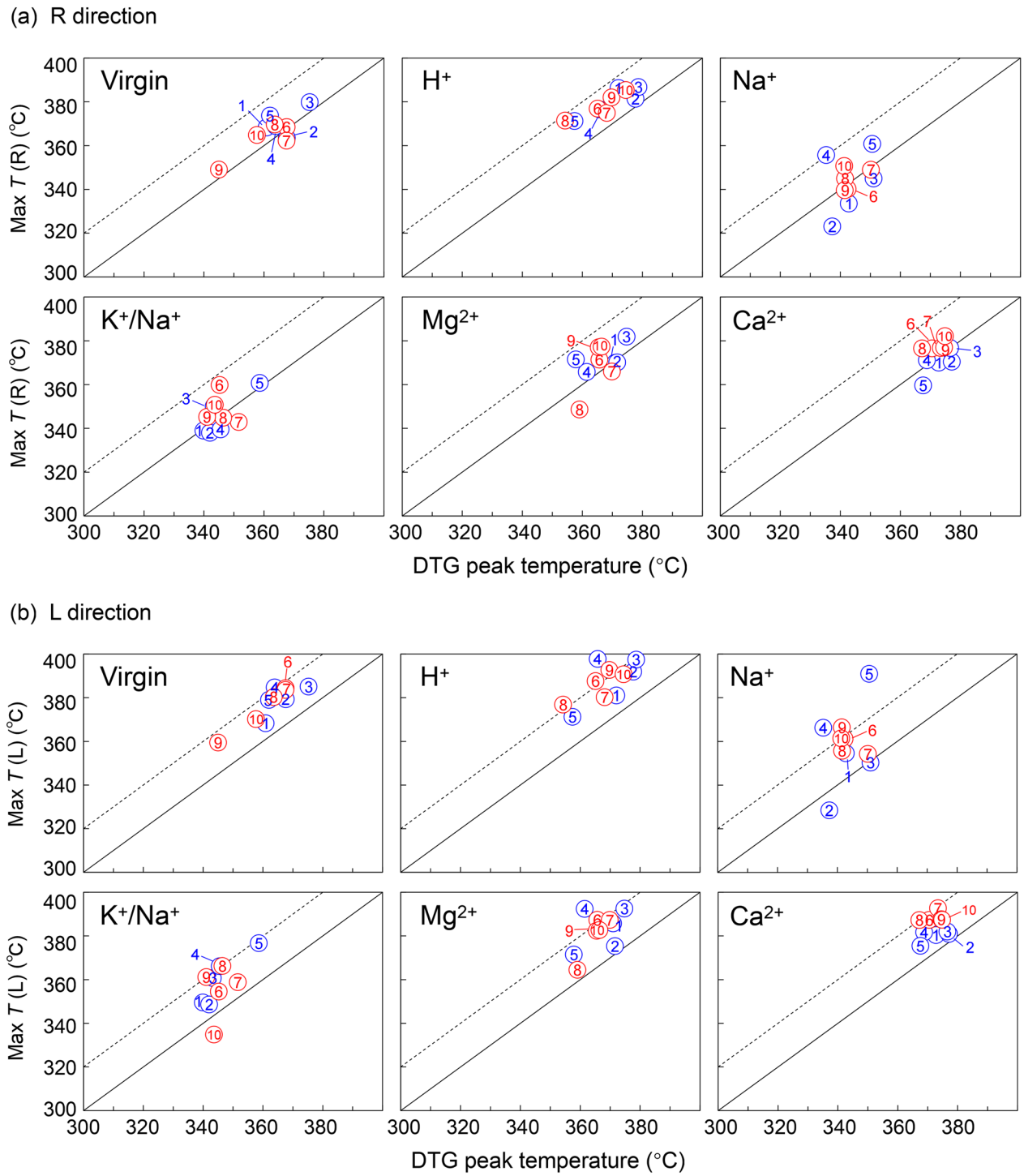


Fig. 6 Peak temperatures of the shrinkage rate curves, Max *T* (R) and Max *T* (L), plotted against the DTG peak temperature (T_p): **a**. R direction; **b**. L direction. Blue: softwoods; red: hardwoods. The solid diagonal line denotes equality, while the dashed line represents T_p + 20 °C for reference

microfibrils structure strongly resists shrinkage in this direction. As observed for the R direction, Max *T* (L) was also higher in H^+- and Mg^{2+}-exchanged samples than in the other cation-exchanged samples.

4 Discussion

Based on these results, the roles of polysaccharide thermal degradation, exchangeable cations, cell types, and species differences in R- and L-direction shrinkage are

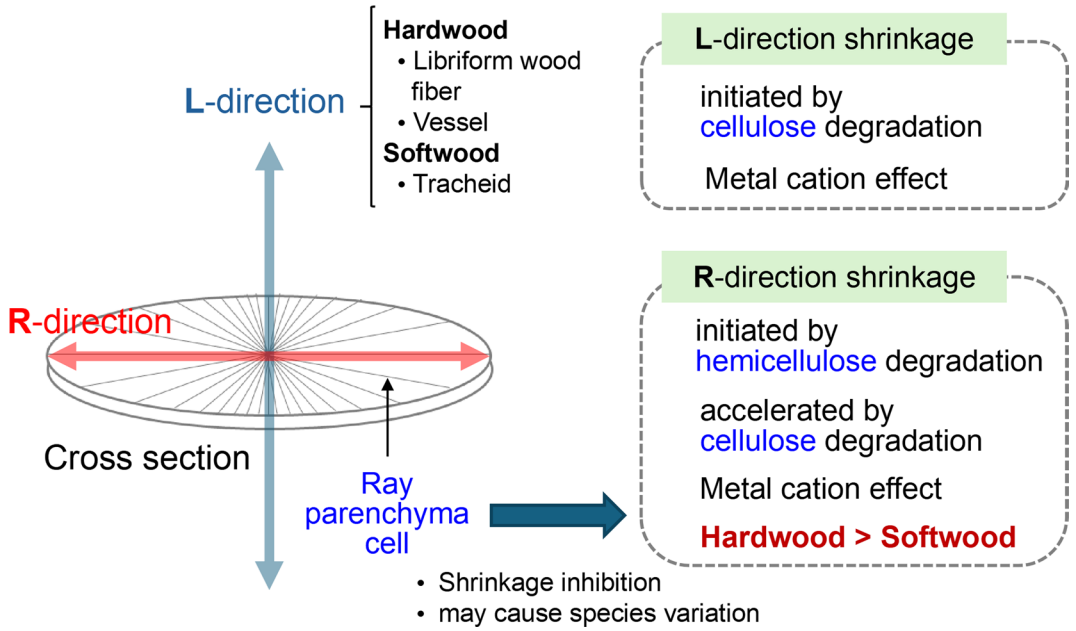


Fig. 7 Schematic illustration of wood cell arrangement for the discussion of the roles of polysaccharide thermal degradation, exchangeable cations, cell types, and species differences in radial and longitudinal shrinkage

discussed with reference to Fig. 7, which schematically illustrates wood cell arrangement. Although lignin pyrolysis behavior may also influence shrinkage, it is not included in the present discussion because quantifying lignin remaining in wood char is challenging.

Lignin generates a smaller amount of volatile products upon pyrolysis compared with cellulose and hemicellulose, and its content in wood is relatively low (approximately 20–30%). Therefore, its influence on shrinkage during carbonization is considered to be less significant than that of cellulose and hemicellulose. Using thermogravimetry–mass spectrometry (TG-MS), we demonstrated that in situ analysis of lignin pyrolysis in wood can be achieved by monitoring volatile products generated during heating (Taira et al. 2026). Our previous study using this method (Wang et al. 2025b) indicated that a fraction of lignin undergoes pyrolysis concurrently with cellulose in all cation-exchanged softwoods and hardwoods, suggesting the co-degradation of cellulose and lignin. Although lignin pyrolysis in wood may promote cellulose degradation, the underlying mechanisms remain unclear. This issue is currently under investigation.

Shrinkage in the R direction began mainly with hemicellulose degradation, with large R-direction shrinkage occurring near the DTG peak temperature as cellulose degradation became significant. In contrast, L-direction shrinkage started around the DTG peak temperature and progressed substantially only after most cellulose had decomposed, reflecting the supramolecular architecture of the cell wall and the longitudinal orientation of cells.

Cellulose microfibrils, aligned along the cell's longitudinal axis (Fengel and Wegener 2011; Ross 1999; Sjöström 2013), resist shrinkage until most have degraded. In the transverse axis, microfibrils are embedded in a hemicellulose–lignin matrix, so shrinkage begins once the hemicelluloses in the matrix degrade. These structural differences explain the contrasting shrinkage behaviors in the R and L directions.

Most cells oriented in the R direction are ray parenchyma (Carlquist 2012; Słupianek et al. 2021; Nakaba and Funada 2024), which resist shrinkage along their long axis; thus, their shape and arrangement strongly influence R-direction shrinkage. In softwoods, they typically occur as single rows along the R direction, whereas in hardwoods they often form large aggregates (Panshin and de Zeeuw 1981; Rowell 2005), as in the multiseriate rays of Japanese beech. Their extremely short long axes, especially in hardwoods (Fengel and Wegener 2011; Ross 1999), may make them more susceptible to shrinkage during thermal degradation, partly explaining the greater R-direction shrinkage of hardwoods. In softwoods, ray tracheids (Wheeler et al. 1989; Rowell 2005) at the ends of ray aggregates may further suppress shrinkage. Although further study is needed, these features highlight the importance of ray parenchyma morphology in controlling R-direction shrinkage.

Among hardwoods, R-direction shrinkage varied by species, with Japanese beech and Japanese walnut showing greater shrinkage, possibly due to their diffuse-porous vessel arrangement (Rowell 2005); large vessel lumens may facilitate inward shrinkage.

In the L direction, most cells (tracheids in softwoods; libriform fibers and vessels in hardwoods) align their long axes along this direction (Bowyer et al. 2003; Rowell 2005; Wheeler et al. 1989), so shrinkage occurs via contraction along the cellulose microfibrils. Because some microfibrils remain until most cellulose has degraded, rapid L-direction shrinkage is observed at $T_p + 10–20$ °C. Above 400 °C, when cellulose degradation is complete, longitudinal restraint is removed and shrinkage anisotropy disappears in charcoal.

The thermal degradation reactivity of cellulose varies with the species of exchangeable cations; substitution with monovalent alkali metals (Na^+, K^+) lowers the degradation temperature by ~30 °C, markedly affecting the shrinkage temperature during carbonization. The present results also suggest that cations influence shrinkage magnitude, likely by altering the thermal degradation, fluidization, and solidification behavior of wood constituents.

Although the present study focuses on elucidating the fundamental mechanisms governing shrinkage during carbonization, the findings also provide a scientific basis for the development of predictive frameworks for biochar production. In particular, understanding how polysaccharide degradation reactivity, exchangeable cation species, and cell structure collectively influence shrinkage behavior may contribute to predicting structural evolution and biochar properties during carbonization. Such mechanistic knowledge may support the rational optimization of feedstock selection, pretreatment strategies, and carbonization conditions. Recent advances in artificial intelligence and machine learning (Chatterjee et al. 2025; Stefko et al. 2025; Kliestik et al. 2024) may further enhance the development of data-driven approaches for predicting complex carbonization behaviors and biochar characteristics. Integrating mechanistic understanding with such predictive methodologies could improve the reliability and applicability of future biochar design and production strategies.

Beyond process optimization, a better understanding of shrinkage and structural evolution during carbonization may facilitate the design of biochars with tailored pore structures and functionalities for specific applications, including environmental remediation and soil improvement (Marousek et al. 2026). Such mechanistic insights may ultimately contribute to more efficient and sustainable biochar production and utilization pathways (Vochozka et al. 2016; Minofar et al. 2025).

In conclusion, this study clarifies how polysaccharide degradation reactivity, exchangeable cation species, and cell structure collectively govern R- and L-direction shrinkage during carbonization. These findings provide new mechanistic insights into anisotropic shrinkage and contribute to a better understanding of micropore and fine-structure formation during biochar production.

5 Conclusions

This study confirms the hypothesis that anisotropic shrinkage during wood carbonization is governed primarily by the sequential thermal degradation of cell-wall polysaccharides and is further modulated by the chemical environment within the cell wall. The results demonstrate that radial and longitudinal shrinkage are not independent phenomena but represent distinct structural responses associated with different stages of polysaccharide decomposition.

A key finding is that the anisotropy of shrinkage progressively diminishes as cellulose-derived structural constraints are lost during carbonization, indicating that cellulose microfibrils play a fundamental role in maintaining dimensional stability at elevated temperatures. Furthermore, the strong influence of exchangeable cations reveals that shrinkage behavior can be manipulated through modification of the cell-wall chemical environment, providing a previously underexplored pathway for controlling carbonization-induced structural evolution.

These findings establish a mechanistic framework linking biomass chemistry, cell-wall structure, and dimensional evolution during carbonization. The proposed hypothesis that both polysaccharide degradation and cation-mediated chemical interactions govern shrinkage behavior is therefore strongly supported by the experimental evidence.

From an application perspective, the results suggest that targeted selection of feedstock species and chemical pretreatments may enable control of shrinkage behavior and consequently influence pore development, microstructure formation, and product quality during biochar production. Such knowledge may contribute to the design of advanced biochar and biomass-derived carbon materials with tailored structural properties for environmental, energy-storage, and carbon-utilization applications.

Supplementary Information

The online version contains supplementary material available at https://doi.org/10.1007/s42773-026-00661-5.

Additional file 1

Acknowledgements
We thank the China Scholarship Council (CSC) for supporting Yu Wang (202204910132) to conduct the present research at Kyoto University.

Author contributions
Writing—original draft, Methodology, Investigation, Formal analysis, Data curation by Yu Wang. Data curation by Ramadan Eljamal, Misao Yokoyama, and Takashi Nomura. Writing—review and editing, Visualization by Eiji Minami. Writing—review and editing, Supervision, Resources, Project administration, Methodology, Funding acquisition, Conceptualization by Haruo Kawamoto. All authors read and approved the final manuscript.

Funding
This work was financially supported by the JST-Mirai Program, Japan (grant number JPMJMI20E3) and a Grant-in-Aid for Scientific Research (A) (No. 22H00381, 2022.4–2026.3; No. 26H02338, 2026.4–2030.3), supported by the Ministry of Education, Culture, Sports, Science and Technology, Japan.

Data availability
The datasets used or analyzed during the current study are available from the corresponding author upon reasonable request.

Declarations

Competing interests
The authors have no relevant financial or non-financial interests to disclose.

Author details
[1]Graduate School of Energy Science, Kyoto University, Yoshida-honmachi, Sakyo-ku, Kyoto 606-8501, Japan.

Received: 9 September 2025 Revised: 15 September 2026 Accepted: 29 September 2026
Published online: 21 October 2026

References

Bowyer JL, Shmulsky R, Haygreen JG (2003) Forest products and wood science. Blackwell, Hoboken
Carlquist S (2012) How wood evolves: a new synthesis. Botany (Ottawa) 90(10):901–940. https://doi.org/10.1139/b2012-048
Chatterjee S, Kliestik T, Rowland Z, Bugaj M (2025) Immersive collaborative business process and extended reality-driven industrial metaverse technologies for economic value co-creation in 3D digital twin factories. Oeconomia Copernicana 16(1):125–161. https://doi.org/10.24136/oc.3596
de Oliveira LJ, Cáceres CB, Hernández RE, Garcia RA (2022) Effect of the thermal treatment on the chemical components, sorption, and shrinkage properties of *Tectona grandis* juvenile wood. Maderas Cienc Technol 24(18):1–16. https://doi.org/10.4067/s0718-221x2022000100418
Fengel D, Wegener G (2011) Wood: chemistry, ultrastructure, reactions. De Gruyter, New York
Gao YF, Fu ZY, Zhou YD, Gao X, Zhou F, Cao HM (2022) Moisture-related shrinkage behavior of wood at macroscale and cellular level. Polymers (Basel) 14(22):5045. https://doi.org/10.3390/polym14225045
Kliestik T, Kral P, Bugaj M, Durana P (2024) Generative artificial intelligence of things systems, multisensory immersive extended reality technologies, and algorithmic big data simulation and modelling tools in digital twin industrial metaverse. Equilib Q J Econ Econ Policy 19(2):429–461. https://doi.org/10.24136/eq.3108
Marousek J, Gavurova B, Maroušková A, Minofar B (2026) Exfoliated biochar activates soil microbial metabolism and demonstrates immobilization potential toward toxic metals and metalloids. Syst Microbiol Biomanuf 6(3):89. https://doi.org/10.1007/s43393-026-00495-z
Maroušek J, Trakal L (2022) Techno-economic analysis reveals the untapped potential of wood biochar. Chemosphere 291:133000. https://doi.org/10.1016/j.chemosphere.2021.133000
Minofar B, Milčić N, Maroušek J, Gavurová B, Maroušková A (2025) Understanding the molecular mechanisms of interactions between biochar and denitrifiers in N_2O emissions reduction: pathway to more economical and sustainable fertilizers. Soil Tillage Res 248:106405. https://doi.org/10.1016/j.still.2024.106405
Nakaba S, Funada R (2024) Cell death of long-lived ray parenchyma cells during heartwood formation in trees. J Wood Sci 70(1):46. https://doi.org/10.1186/s10086-024-02160-2
Panshin AJ, de Zeeuw C (1981) Textbook of wood technology. McGraw Hill, New York
Rafsanjani A, Stiefel M, Jefimovs K, Mokso R, Derome D, Carmeliet J (2014) Hygroscopic swelling and shrinkage of latewood cell wall micropillars reveal ultrastructural anisotropy. J R Soc Interface 11(95):20140126. https://doi.org/10.1098/rsif.2014.0126
Ross RJ (1999) Wood handbook: wood as an engineering material, vol vol 113. Forest Products Research, Madison
Rowell RM (2005) Handbook of wood chemistry and wood composites. CRC Press, Boca Raton
Sjöström E (2013) Wood chemistry: fundamentals and applications. Academic Press, New York
Słupianek A, Dolzblasz A, Sokołowska K (2021) Xylem parenchyma—role and relevance in wood functioning in trees. Plants (Basel) 10(6):1247. https://doi.org/10.3390/plants10061247
Stefko R, Frajtova-Michalikova K, Strakova J, Novak A (2025) Digital twin-based virtual factory and cyber-physical production systems, collaborative autonomous robotic and networked manufacturing technologies, and enterprise and business intelligence algorithms for industrial metaverse. Equilib Q J Econ Econ Policy 20(1):389–425. https://doi.org/10.24136/eq.3557
Taira D, Nomura T, Minami E, Kawamoto H (2026) In situ assessment of lignin pyrolysis reactions and their interactions with polysaccharides in Japanese cedar wood cell walls by TG-MS and Py-GC/MS. J Anal Appl Pyrolysis 195:107638. https://doi.org/10.1016/j.jaap.2026.107638
Vochozka M, Maroušková A, Váchal J, Straková J (2016) The economic impact of biochar use in Central Europe. Energy Sources A 38(16):2390–2396. https://doi.org/10.1080/15567036.2015.1072600
Wang P, Howard BH (2017) Impact of thermal pretreatment temperatures on woody biomass chemical composition, physical properties and microstructure. Energies 11(1):25. https://doi.org/10.3390/en11010025
Wang Y, Nomura T, Eljamal R, Minami E, Kawamoto H (2024) Thermogravimetric investigation of anisotropy of dimensional shrinkage of softwood and hardwood during carbonization. Wood Sci Technol 58(3):959–974. https://doi.org/10.1007/s00226-024-01560-3
Wang Y, Eljamal R, Nomura T, Minami E, Kawamoto H (2025a) Thermal reactivities of hemicellulose and cellulose and demineralization effects on their reactivities in cell walls of various softwood and hardwood species. J Wood Sci 71(1):39. https://doi.org/10.1186/s10086-025-02216-x
Wang Y, Taira D, Eljamal R, Nomura T, Minami E, Kawamoto H (2025b) Cation-exchangeable metal cations govern the thermal reactivity of hemicellulose and cellulose across wood species: implications for cell wall ultrastructure. Ind Crops Prod 234:121599. https://doi.org/10.1016/j.indcrop.2025.121599
Wheeler EA, Baas P, Gasson PE (1989) IAWA list of microscopic features for hardwood identification. National Herbarium of the Netherlands, Leiden
Xue Q, Sun W, Fagerstedt K, Guo X, Dong M, Wang W, Cao H (2018) Effects of wood rays on the shrinkage of wood during the drying process. BioResources 13(3):7086–7095. https://doi.org/10.15376/BIORES.13.3.7086-7095
Yu M, Saunders T, Su T, Gucci F, Reece MJ (2018) Effect of heat treatment on the properties of wood-derived biocarbon structures. Materials (Basel) 11(9):1588. https://doi.org/10.3390/ma11091588